Suppressing Recombination in Polymer Photovoltaic Devices via Energy-Level Cascades

*Zhi-Kuang Tan, Kerr Johnson, Yana Vaynzof, Artem A. Bakulin, Lay-Lay Chua, Peter K. H. Ho, and Richard H. Friend**

Efficient photogeneration of charge carriers and suppression of their recombination are two of the key challenges facing organic photovoltaic systems. These challenges are addressed in photosynthetic systems by the use of energy cascades,[1,2] through which the electron and hole are rapidly spatially separated, thus suppressing their recombination. Here we demonstrate that an analogous energy cascade can be implemented at the polymer donor–polymer acceptor heterojunction through the use of a thin (0.5–4 nm) polymer interlayer with intermediate highest-occupied-molecular-orbital (HOMO) and intermediate lowest-unoccupied-molecular-orbital (LUMO) energy levels. This layer was fixed in place by a fluorinated bis(phenyl azide) photo-crosslinking methodology.[3] We used regioregular poly(3-hexylthiophene) (P3HT) as the electron donor, poly{[N,N′-bis(2-octyldodecyl)-naphthalene-1,4,5,8-bis(dicarboximide)-2,6-diyl]-*alt*-5,5′-(2,2′-bithiophene)} (P(NDI2OD-T2)) as the electron acceptor, and poly[N-9′′-hepta-decanyl-2,7-carbazole-*alt*-5,5-(4′,7′-di-2-thienyl-2′,1′,3′-benzothiadiazole)] (PCDTBT) as the interlayer. Using an optimal interlayer thickness of 3 nm, our modified device yielded an almost two-fold increase in power conversion efficiency from 0.26% to 0.45%, comparable to the good performance found in related P3HT/fullerene bilayers.[4] Dark current and ultrafast spectroscopy measurements confirm that the interlayer blocks the recombination of charges that are either injected or photogenerated across the cascade. These findings open new routes for photovoltaic performance optimization by reducing recombination losses across the donor-acceptor interface, and offer scope to replace the "workhorse" fullerenes with polymeric acceptors.

Z.-K. Tan, K. Johnson, Dr. Y. Vaynzof,
Prof. R. H. Friend
Cavendish Laboratory
University of Cambridge
JJ Thomson Avenue, Cambridge CB30HE, UK
E-mail: rhf10@cam.ac.uk
Dr. A. A. Bakulin
FOM institute AMOLF
Science Park 104, Amsterdam, The Netherlands
Dr. L.-L. Chua
Department of Chemistry
National University of Singapore
Lower Kent Ridge Road, S117543, Singapore
Prof. P. K. H. Ho
Department of Physics
National University of Singapore
Lower Kent Ridge Road, S117542, Singapore

DOI: 10.1002/adma.201300243

The field of organic photovoltaics has seen significant advancements since the invention of the donor-acceptor organic bulk heterojunction.[5,6] Recent work has suggested a clear path forward to optimize the morphology of the donor–acceptor heterostructure using selective crosslinking to provide the appropriate path continuities of the electron and hole transport phases.[3] However, there is little work yet on the development and implementation of the appropriate energy levels to improve photocarrier generation yields while suppressing recombination. In conventional understanding, imposing the appropriate energy offsets between the HOMO/LUMO of the donor and that of the acceptor phases drives the dissociation of the photogenerated exciton, to produce electron-hole pairs which may either separate or relax to form bound charge transfer (CT) states across the heterojunction interface.[7] Many polymer donor–fullerene acceptor systems show very efficient charge separation,[8,9] but in contrast, polymer-polymer systems show poor efficiencies, with formation of CT states that are bound at room temperature and are further limited by a large bimolecular recombination coefficient.[10] Therefore, charge recombination, both geminate[11–14] and non-geminate,[9,15,16] severely limits the performance of many polymer organic solar cell devices that have been investigated.

Photosynthetic systems employ a sequence of cascade steps to dissociate the exciton, thereby giving a spatially separated electron–hole pair on rapid time scales while blocking recombination to achieve a near unity charge separation quantum yield.[1,2] This has, over the years, inspired studies of ternary blend bulk heterojunction solar cells, which may in principle form ordered, cascaded structures.[17–20] However, these studies have yet to demonstrate the cascade structure and devices show modest PV performance.

In this paper, we demonstrate that the principle of energy-level cascades can be implemented in an all-polymer solar cell using a completely solution-processed technique. The results reveal that a through-space coupling of the energy levels of the donor and acceptor levels via a thin interlayer can be remarkably effective in achieving exciton dissociation and suppressing charge recombination, thereby giving a significant enhancement in the photocarrier generation yield.

As shown in **Figure 1**a, we used the P3HT/P(NDI2OD-T2) pair as the all-polymer donor/acceptor system[21] and PCDTBT as the thin interlayer modifier. The ionization potentials of P3HT, PCDTBT and P(NDI2OD-T2) were determined to be 4.7, 5.1, and 5.4 eV respectively by ultraviolet photoelectron

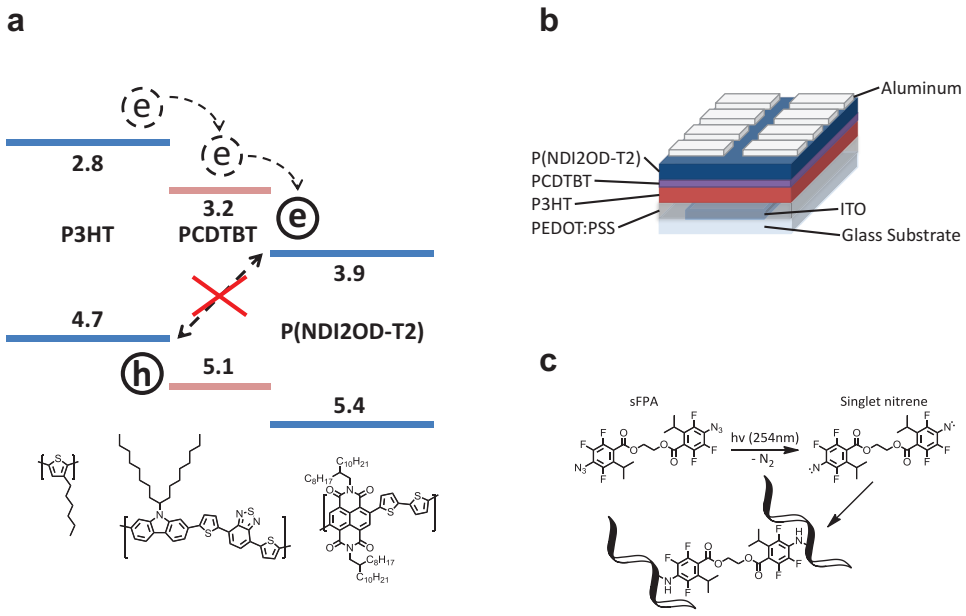

Figure 1. a) Cascading energy levels of donor and acceptor polymers with thin interlayer. b) Device structure of ITO/PEDOT:PSS/P3HT/PCDTBT/P(NDI2OD-T2)/Al in polymer photovoltaic device. c) Reaction schematic for the photo-crosslinking of polymer chains with sFPA.

spectroscopy (UPS) and the electron affinities were estimated to be 2.8, 3.2, and 3.9 eV using the optical bandgaps measured from their absorption onset (note that we make no allowance here for exciton binding energy). This gives the desired energy-level cascade.

The devices were fabricated in the conventional structure of ITO/PEDOT:PSS/P3HT/PCDTBT/P(NDI2OD-T2)/Al as illustrated in Figure 1b. The planar multi-layered structures were created by sequential photo-crosslinking, developing and solution spin-casting steps. Photo-crosslinking rendered the underlying polymer layer insoluble, hence allowing the deposition of the top layers by solution processing without the need for orthogonal solvents. We used ethylene bis(4-azido-2,3,5-trifluoro-6-isopropylbenzoate), a sterically substituted ultraviolet-active bis(fluorophenyl azide) (sFPA) that we have recently developed, for the purpose of photo-crosslinking.[3] The reaction schematic of the photo-crosslinking process is shown in Figure 1c. The key to its success is the non-specific photo-crosslinking mechanism, which enables small amounts of the photo-crosslinker to be used, close to theoretical minimum, to achieve highly efficient crosslinking of the polymer above its gel point. Under our experimental conditions, the gelation fraction was around 60%. Furthermore, the crosslinking mechanism is dominated by alkyl side-chain insertions, which do not alter the (opto)electronic properties of the π-conjugated cores.[3]

The thickness of each polymer layer was determined from the optical density of the layer, calibrated by atomic force microscopy (AFM). P3HT was prepared with a thickness of 13 nm, a little larger than the reported exciton diffusion length of 8.5 nm.[22,23] Varying thicknesses of PCDTBT (between 0.5 and 4.0 nm) were deposited on top of P3HT to study the influence of the interlayer on device performance. For details on PCDTBT thin film deposition and AFM images of the films, see supplementary information. The top-most layer of P(NDI2OD-T2) was made thicker, at 36 nm, to avoid shunts between the two electrodes. We note that 36 nm is likely to be much greater than the exciton diffusion length, and only the excitons near to the planar heterojunction would be able to contribute to photocurrent.

We performed photoemission spectroscopy measurements of both the valence and core electronic levels in order to assess the quality of the surface coverage of PCDTBT over the underlying P3HT layer. **Figure 2**a follows the evolution of the valence band, as measured by ultraviolet photoemission spectroscopy (UPS), of films with increasing PCDTBT thickness deposited on top of crosslinked P3HT film. As the spectra are shown as a function of binding energy with respect to the vacuum level, the low energy edge of the valence band corresponds to the position of the HOMO and determines the ionization potential (IP) of the polymer film.[24] For a bare P3HT film, we measured the IP to be 4.7 eV, in good agreement with previous reports.[25] For the 0.5 nm, 1 nm, and 2 nm thick PCDTBT overlayers, we observed an increase in the PCDTBT valence band features, which are superimposed on a P3HT valence band structure. This implies incomplete coverage of the P3HT layer. The UPS spectra for the 3 nm and 4 nm thick PCDTBT overlayers are, in contrast, fully dominated by the PCDTBT valence band structure. Because the inelastic mean free path at these kinetic energies in organic thin films is very small (ca. 0.6 nm), the results demonstrate that complete coverage by the PCDTBT polymer first emerges at a nominal thickness of 3 nm. This shows that stiff conjugated polymer chains can form continuous films with substantially extended chains at thicknesses of a few monolayers.[26] The spectrum of a pure PCDTBT polymer film is shown for reference and the IP of these overlayers matched the measured IP of the pure PCDTBT film at 5.1 eV.

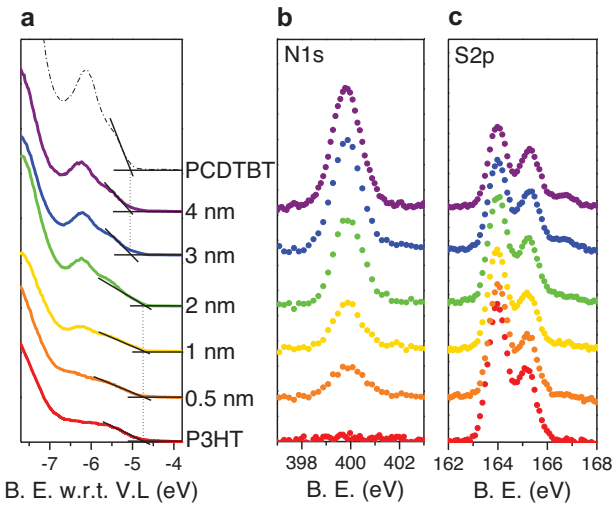

Figure 2. a) UPS-measured valence-band spectra of various thicknesses of PCDTBT overlayers on P3HT film as a function of binding energy with respect to the vacuum level. A spectrum of a pure PCDTBT film is shown for reference. b,c) N1s (b) and S2p (c) XPS spectra of various thicknesses of PCDTBT overlayers on a P3HT film. The PCDTBT overlayers were photo-crosslinked and spin-rinsed with chlorobenzene to remove unbound fractions prior to photoemission measurements.

Figure 2b,c present the results of X-ray photoemission spectroscopy (XPS) measurements of the N1s and S2p spectral regions. As expected, the N1s signal increased with increasing thickness of the PCDTBT layer as only the benzothiadiazole (BT) units of the PCDTBT polymer contain N atoms. The S2p spectra evolved from a single spin-orbit ($S2p_{3/2}$–$S2p_{1/2}$) doublet, corresponding to the S atoms from P3HT, to a twin doublet due to the additional contribution of the S from the BT unit in PCDTBT. This is particularly clear for the 3 nm and 4 nm thick overlayer films.

These experiments demonstrate unambiguously that a continuous thin film of the PCDTBT polymer can be fabricated over the crosslinked P3HT layer, and this overlayer, when crosslinked, is itself robust to further solvent processing. Furthermore, we note that when the PCDTBT layer is deposited over the crosslinked P3HT underlayer, swelling of the underlying crosslinked P3HT layer occurs, as expected because chlorobenzene is a good solvent for P3HT. This swelling–deswelling cycle could promote partial intermixing at the interface. From the emergence of complete coverage at 3 nm in the UPS measurements, we infer a diffuse interface of thickness of the order of 1–2 nm. Using photoluminescence studies, we confirmed that the PCDTBT did not penetrate further into the bulk of P3HT (see supplementary information).

We fabricated photovoltaic devices that incorporate various thicknesses of the PCDTBT interlayers to investigate the photocarrier generation efficiency of these structures. In our devices, we obtained a significant increase in both photocurrent generated and also in the open-circuit voltage (V_{oc}) upon the insertion of the interlayer, as shown in the current density-voltage curve in **Figure 3**a. The short-circuit current density (J_{sc}) increases from 0.86 mA cm^{-2} in devices with no interlayer, to level off at 1.23 mA cm^{-2} in devices with 4 nm interlayer, under simulated AM1.5G illumination. A significant increase in J_{sc} to 1.09 mA cm^{-2} (27% increase) was found with an insertion of only 0.5 nm of interlayer, which is on average only one molecular layer thick. The J_{sc} continues to increase gradually beyond 0.5 nm interlayer thickness and levels off at about 4 nm. These increases in short-circuit currents were also reflected in the short-circuit external quantum efficiency (EQE) measurements shown in Figure 3b, where devices with 4 nm interlayer gave 7.6% EQE (at 550 nm) compared to only 5.4% EQE in devices without the interlayer. The contribution to the EQE from P(NDI2OD-T2) (650–850 nm) is small in all cases due to the polymer's small extinction coefficient, which we measure to be a factor of 3 smaller as compared to that of P3HT (see Supporting Information). The general enhancement in photocurrent at all biases demonstrates an increased photocarrier generation yield. We note that there is partial contribution to the photocurrent from photoabsorption in the PCDTBT interlayer. However, this contribution is small for PCDTBT thicknesses below 2 nm, as confirmed by optical transfer matrix calculations.[27,28] Taking the exciton diffusion length in the polymers to be 8.5 nm,[23] we calculate that the PCDTBT absorption for a 0.5 nm interlayer device only contributed to an extra 6% in charge generation (by exciton generation, diffusion and charge transfer at heterojunction), but the corresponding EQE improvement was much higher at 27%. photogeneration from PCDTBT absorption is more evident at 3–4 nm thicknesses (see supplementary information). We also observed a systematic increase in the V_{oc} from 0.58 V in devices with no interlayer, to 0.75 V in devices with the 4 nm interlayer. The combination of improvements in device characteristics gave a remarkable near two-fold increase in power conversion efficiency (PCE) from 0.26% in the unmodified bilayer devices, to 0.45% in devices with 3 nm interlayer (see **Table 1**). We note

Table 1. Summary of Device Characteristics of Polymer Photovoltaic Devices

PCDTBT Thickness	V_{oc}[a] [V]		J_{sc}[a] [mA cm^{-2}]		Fill Factor[a] [%]		PCE[a] [%]	
0 nm	0.583	(±0.005)	0.86	(±0.03)	52.8	(±0.6)	0.26	(±0.01)
0.5 nm	0.626	(±0.005)	1.09	(±0.04)	55.0	(±0.5)	0.37	(±0.02)
1 nm	0.641	(±0.007)	1.13	(±0.03)	54.4	(±0.3)	0.39	(±0.02)
2 nm	0.689	(±0.006)	1.19	(±0.03)	52.6	(±0.4)	0.43	(±0.01)
3 nm	0.727	(±0.003)	1.21	(±0.05)	50.7	(±0.4)	0.45	(±0.02)
4 nm	0.753	(±0.003)	1.23	(±0.04)	47.8	(±0.3)	0.44	(±0.01)

[a]The values in brackets indicate the standard deviations of the measurement over 5–8 devices.

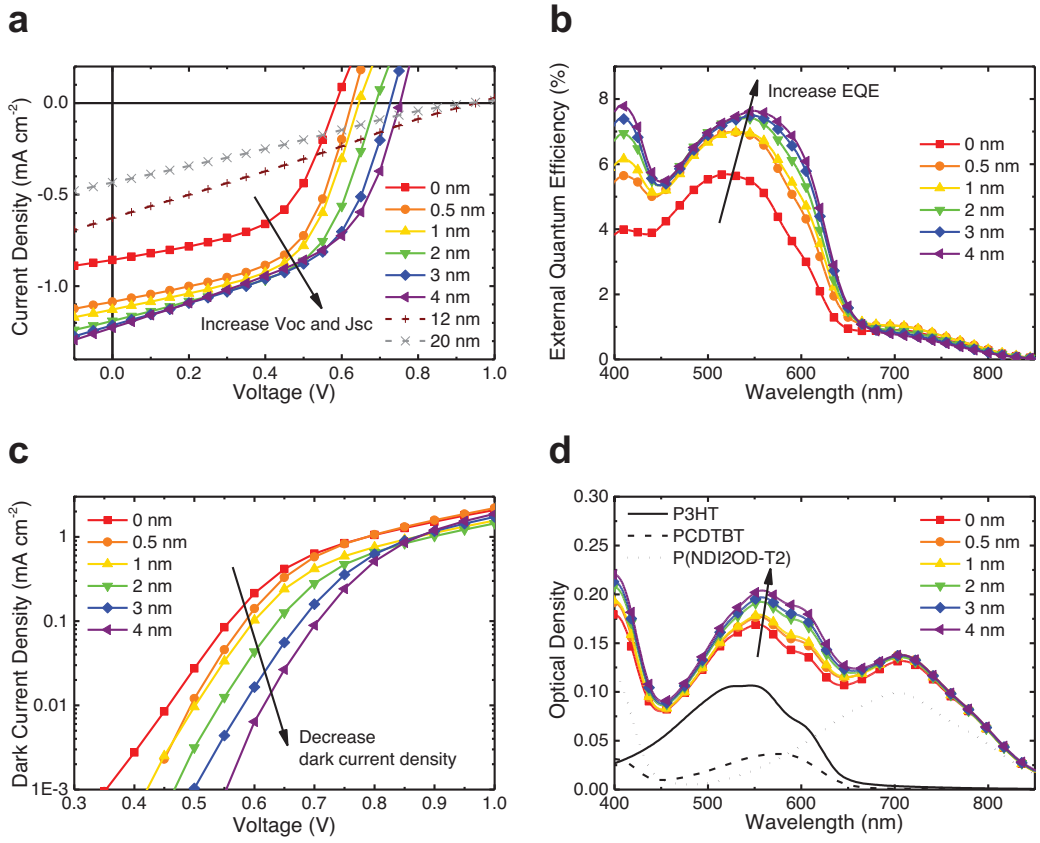

Figure 3. Device characteristics of polymer photovoltaic devices. a) Current density versus voltage characteristics of ITO/PEDOT:PSS/P3HT(13 nm)/PCDTBT/P(NDI2OD-T2)(36 nm)/Al devices under simulated AM1.5G illumination. b) Short-circuit external quantum efficiency spectra of devices. c) Current density versus voltage characteristics of devices in the dark. d) Optical density of polymer active layer in the devices, with pure polymer films shown as reference. The values in the legend represent the thickness of the PCDTBT interlayer.

that the efficiencies obtained in our modified all-polymer P3HT-based devices are comparable to reported efficiencies of P3HT/fullerene bilayer systems,[4] which generally possess close to unity photogeneration yield.[8]

To investigate the possibilities of recombination suppression as the mechanism behind improved device performance, we measured the current density-voltage characteristics of the modified devices in the dark. As clearly seen in Figure 3c, devices with the interlayer recorded a significantly lower dark current density under forward biases, which was up to 2 orders of magnitude smaller compared to the dark current in unmodified devices. We consider that the dark current under forward bias must be controlled by the recombination of electrons and holes at the polymer heterojunction interface and that injection/extraction from the anode and cathode does not limit current density. For the single heterojunction in the P3HT/P(NDI2OD-T2) device, electron-hole capture is effective and the dark current is therefore high. In contrast, in the presence of the interlayer, this recombination process is blocked. We note that the differences in dark current density could not have resulted from any changes in the carrier injection efficiencies since the polymer-electrode interfaces were the same in all devices.

Transient optical spectroscopy was used to provide further insight into the molecular mechanism of recombination suppression. We studied the charge dynamics in the system with a combination of techniques to cover the early time generation and recombination (0.1 ps to 2 ns) and also the longer time decay (1 ns to 10 μs) that occurs on the timescales for charge transport and non-geminate recombination. For this longer timescale, all-optical transient absorption (TA) spectroscopy was used to monitor the recombination kinetics in the thin-film samples that reproduce the active layers of the devices studied above. TA is the measurement of the differential transmission ($\Delta T/T$) of a sample, and its temporal evolution, after a pump pulse generates new photoexcited species. We used an excitation wavelength of 532 nm, which predominantly excited P3HT. TA spectra were measured over the 525–825 nm range with the signal around 810 nm corresponding to photoinduced absorption of polarons on the polymer chains.[14,29–32] For details, see the Supporting Information.

The photoinduced absorption, reflecting the charge concentration in the film, is shown as a function of time in **Figure 4**a, together with individual P3HT/PCDTBT and PCDTBT/P(NDI2OD-T2) interfaces for reference. The normalized data clearly shows the trend of increasing charge lifetime with increasing PCDTBT interlayer thickness, with the time for the signal to decay (to $1/e$) increasing by almost one

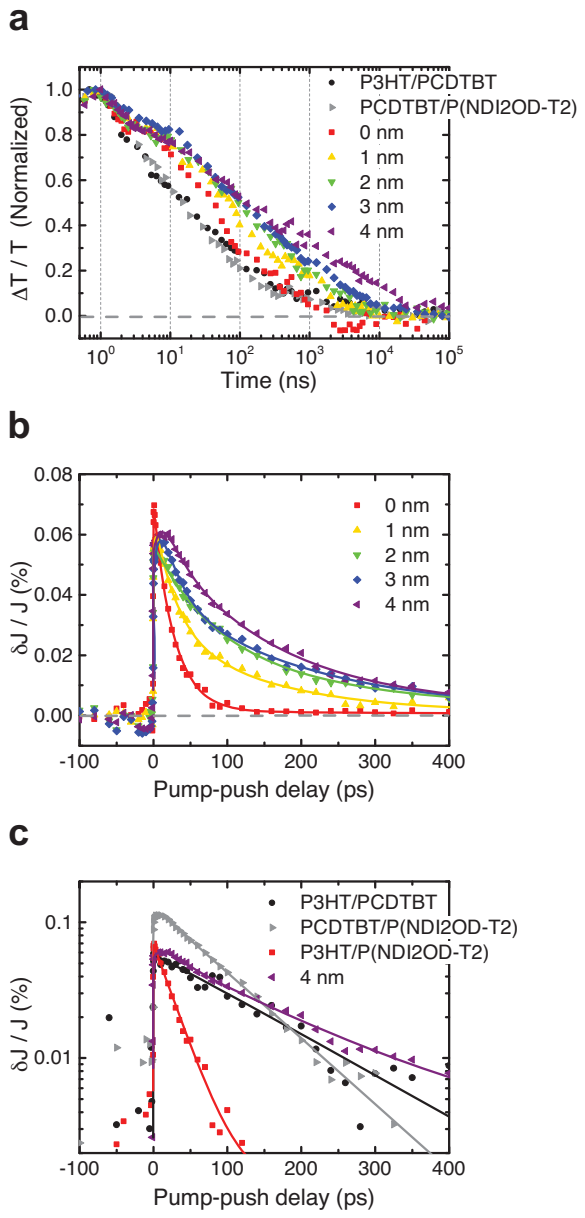

Figure 4. a) Normalized transient absorption kinetics, averaged over 800–820 nm wavelengths, for the range of P3HT (7 nm)/PCDTBT/P(NDI2OD-T2) (15 nm) samples (interlayer thickness indicated) and the reference interfaces described in the text. The excitation wavelength is 532 nm. b) Relative concentration of interfacial bound charge pairs as a function of time, observed in pump-push photocurrent experiments performed on P3HT (13 nm)/PCDTBT/P(NDI2OD-T2) (36 nm) cells with different interlayer thickness and (c) on P3HT (13 nm)/PCDTBT (4 nm), PCDTBT (4 nm)/P(NDI2OD-T2) (36 nm) and P3HT (13 nm)/P(NDI2OD-T2) (36 nm) bilayer reference devices. The solid lines are multiexponential fits to the data. The pump and push wavelengths are 600 nm and 2200 nm respectively.

order of magnitude from ≈60 ns to ≈400 ns when a 3–4 nm interlayer is present. The charge pairs generated across the P3HT/PCDTBT and the PCDTBT/P(NDI2OD-T2) reference interfaces both decay faster than the charge pairs in the P3HT/PCDTBT/P(NDI2OD-T2) films. This rules out an interface specific effect whereby one of the interfaces may be the cause of an increased charge lifetime. The increase in lifetime, only when PCDTBT interlayer is present, confirms the suppression of electron–hole recombination across the stack.

At short timescales, the same TA measurement is complicated by early-time non-linear response and by the several overlapping absorption features of the three polymers. Hence, we used instead the "CT state only" sensitive "pump-push" photocurrent spectroscopy that we have recently developed.[33,34] In this experiment, a working photovoltaic device is first exposed to an above bandgap (≈600 nm) pump pulse which generates photocarriers (and related photocurrent J) as well as bound CT states. This is followed by a second infrared (IR) pulse, in the region of the hole polaron absorption band (0.56 eV), after a variable time delay. For those charges that were bound in an interfacial CT state, this "push" pulse provides an extra chance of release and thus causes additional photocurrent δJ. Therefore, $\delta J/J$ reflects the variations in the relative amount of CT states at the interface, as a function of delay after the initial photoexcitation event.

The pump-push photocurrent transients, recorded for interlayer-modified devices and the reference bilayer devices under the short-circuit condition, are shown in Figure 4b and c respectively. Devices with interlayers show a gradual switch, with increasing PCDTBT thickness, from the shortest time response of 30 ps for the P3HT/P(NDI2OD-T2) device to 170 ps for the 4 nm interlayer device. Since both P3HT/PCDTBT and PCDTBT/P(NDI2OD-T2) reference devices have long response times of 150 ps and 100 ps respectively, it is possible that these pump-push responses are due to CT states that form at one of the two heterojunctions (more likely with P3HT/PCDTBT since this has the longer response). The disappearance of the fast-decay component for 3–4 nm interlayer devices is certainly consistent with the photoemission data, which shows that the P3HT/P(NDI2OD-T2) interface is no longer present and full coverage is achieved at 3 nm. The max $\delta J/J$ amplitude is comparable in size for all devices. This indicates that the proportion of CT states formed at early-times (<1 ps) does not change markedly with interlayer modifications, implying that the initial step of charge generation (i.e., charge transfer into bound CT-states or separation into free charges) across the interface is not significantly altered. We therefore conclude that the improvement in quantum efficiency does not result primarily from a better early-time charge separation (which is probably reasonably efficient in all cases), but rather from the suppression of later time recombination as shown in Figure 4a. The suppression of recombination is also consistent with the increase in open-circuit voltage described above.[9] The open-circuit voltage is the voltage at which the recombination current equals and offsets the photogeneration current. When recombination is switched off, higher current collection is possible at all voltage biases, which necessarily gives a higher open-circuit voltage.

In order to validate that the device improvements originated from the interface modification, and not from the bulk doping of P3HT during the solution processing steps, we repeated our experiments using inverted device structures of indium tin oxide (ITO)/ZnO/P(NDI2OD-T2)/PCDTBT/P3HT/WO_3/Ag.

In our inverted devices, PCDTBT was solution deposited on top of crosslinked P(NDI2OD-T2), and was not expected to cause bulk doping of the P3HT layer. We found our inverted devices to exhibit the similar trends of increases in V_{oc}, J_{sc} and EQE with increasing interlayer thicknesses (see Supporting Information).

We note that the optimum interlayer thickness is 3 nm for both the standard and the inverted devices, which is the thickness where full coverage is first achieved. The short-circuit current improves with increasing coverage of interlayer up to 4 nm, but performance drops notably above that (see Figure 3a). We can presume that for the thicker devices, the two heterojunctions function independently, and that the poor photovoltaic response results from recombination at each of the heterojunctions and transport-related losses. In contrast, for thinner interlayers of 3 nm or less, the two heterojunctions function cooperatively, with some level of coherent electronic coupling between them. We note that the PCDTBT polymer chains, which we estimate from the crosslinking parameters to have 50 or more repeat units, will almost all bridge across the thickness of the interlayer and be in electronic contact with the upper and lower polymers. We speculate that this allows the coherent transfer of electrons or holes across the interlayer, making use of the relatively delocalized charge wavefunctions on the polymer chains, hence allowing a good increase in short-circuit current with interlayer thicknesses as high as 4 nm. In comparison, devices made using three layers of sequentially evaporated small molecules often show little or no increase of short-circuit current.[35–37] In those instances where an increase in short-circuit current is observed, it is seen for very thin interlayers and drops off noticeably above 1.5 nm interlayer thickness.[38]

The device performance is therefore determined by this interplay between interlayer coverage (increasing coverage improves the recombination blocking effect), cooperation of the double heterojunctions (increasing thickness reduces the efficient cascading of charges across the interlayer) and increased absorption (which increases the number of excitons generated).

Although providing a working proof of concept, the planar-structured energy-cascading devices presented in this study show lower power conversion efficiencies as compared to bulk-heterojunction structures.[21] In order to fabricate high efficiency devices, a bulk structure is needed to provide high surface area for exciton dissociation into charges. Our solution-processed technique provides scope for making bulk-cascade structures using well-established nano-imprinting methods[39–41] and phase-director methods.[3] Alternatively, one could explore restricted demixing via self-assembly of a triblock copolymer. If successfully implemented in a bulk heterojunction, such energy-level cascading design may match or surpass the performance of the superior polymer-fullerene systems.

We have demonstrated an elegant approach to improve polymer photovoltaic device performance through engineering an energy-level cascade in a simple 3-layered structure. We have also proved with a range of ultrafast techniques and current-voltage studies that the improvements originate from the suppression of recombination at the polymer heterojunction interface. The facile solution processing and photo-crosslinking methods enable such interfacial modifications to be conveniently applied on a large scale in well-defined heterostructures. This work opens up many exciting opportunities to improve the performance of existing polymer photovoltaic systems that are known to suffer from recombination problems,[12,13] and could pave the way towards high-efficiency solar cells with enhanced photocarrier generation yields.

Experimental Section

Materials: P3HT (Rieke Metals, Sepiolid P200), PCDTBT (1-Material), P(NDI2OD-T2) (Polyera) and poly(3,4-ethylenedioxythiophene) poly(styrenesulfonate) (PEDOT:PSS) (Heraeus, Clevios P VP AI 4083) were used as received. sFPA photo-crosslinker was synthesized in-house based on procedures described elsewhere.[3]

Photo-crosslinking: Photo-crosslinking was performed in a nitrogen-filled glovebox at a dose of about 3 J cm^{-2} at 254 nm wavelength from a 6 W low-pressure Hg lamp.

Photovoltaic Device Fabrication: ITO-coated glass substrates were cleaned by successive sonication in acetone and isopropyl alcohol, followed by oxygen plasma treatment. PEDOT:PSS (≈30 nm) was spin-coated onto the substrate, followed by heat annealing at 120 °C for 30 minutes under nitrogen atmosphere. The substrates were transferred into a nitrogen-filled glovebox for further fabrication steps. A solution of P3HT in chlorobenzene, mixed with 10 w% sFPA (w.r.t. the polymer) was spin-coated on top of PEDOT:PSS. The film was heat annealed at 90 °C for 5 minutes, quenched to room temperature, and photoexposed for crosslinking. The crosslinked film was spin-rinsed twice with chlorobenzene solvent to wash away non-crosslinked fractions to give a 13 nm P3HT film. PCDTBT (0–4 nm) was deposited from a solution in chlorobenzene with 5 w% sFPA, following the spin-casting, photo-crosslinking and developing methods described above. Details of the PCDTBT deposition are in the Supporting Information. Finally, a layer of P(NDI2OD-T2) (36 nm) was spin-coated from a solution in chlorobenzene. A 100 nm layer of aluminium was deposited by thermal evaporation under high vacuum (≈10^{-6} mbar). Completed devices were annealed at 120 °C for 10 minutes. All of the devices were encapsulated before device characterization in air.

Inverted Photovoltaic Device Fabrication: ZnO thin film (≈40 nm) was deposited on top of precleaned ITO-coated glass substrates, using chemical spray pyrolysis of 80 g L^{-1} zinc acetate dihydrate solution in methanol. The substrates were transferred into a nitrogen-filled glovebox for further fabrication steps. P(NDI2OD-T2) was spin-coated from a solution in chlorobenzene, mixed with 2.5 w% sFPA. The above described photo-crosslinking and developing methods were followed to obtain a 36 nm P(NDI2OD-T2) film. PCDTBT (0–4 nm) was deposited as described in the section above. P3HT was spin-coated from a solution in chlorobenzene to give a 15 nm film. WO_3 (8 nm) and Ag (100 nm) were successively deposited by high-vacuum thermal evaporation. Completed devices were annealed at 120 °C for 10 minutes and encapsulated before device characterization in air.

Device Characterization: The short-circuit external quantum efficiency (EQE) was measured as a function of wavelength. A 250 W tungsten filament lamp, dispersed through a monochromator, was used as the light source. The incident monochromatic light intensity was monitored using a calibrated reference photodiode and the corresponding short-circuit current at each wavelength was recorded using a Keithley 2635 Source Measure Unit (SMU). The device current-voltage characteristics, under the illumination of an Oriel 81160-1000 solar simulator, were measured using the Keithley 2635 SMU. The solar simulator was calibrated with a silicon reference solar cell, to give an equivalent illumination intensity of 100 mW cm^{-2} AM 1.5G, after correction for spectral mismatch. The UV–vis absorption spectra of the device active layers were acquired using a Hewlett Packard 8453 diode array spectrometer.

Photoemission Spectroscopy: Samples for photoemission spectroscopy (PES) were fabricated on Au/Si substrates. Pure polymer samples were deposited directly onto the substrates by spin-casting to give films of 7-8 nm thicknesses. For samples with a PCDTBT overlayer, P3HT was first deposited to a thickness of 7 nm, followed 0.5–4 nm of PCDTBT, all following the solution casting and photo-crosslinking methods described in the above "Photovoltaic Device Fabrication" section. The photo-crosslinked PCDTBT overlayers were spin-rinsed with chlorobenzene to remove unbound fractions prior to photoemission measurements.

The PES samples were transferred to the ultrahigh vacuum (UHV) chamber (ESCALAB 250Xi) for UPS/XPS measurements. UPS measurements were performed using a double-differentially pumped He gas discharge lamp emitting He I radiation ($h\nu$ = 21.22 eV) with a pass energy of 5 eV. XPS measurements were carried out using a XR6 monochromated X-ray source with a 650 μm spot size.

Transient Absorption Spectroscopy. A Ti:sapphire amplifier system (Spectra-Physics, Solstice) was used to generate a train of 90 fs pulses at 1 kHz. A portion of the 800 nm output was used to pump a home-built broadband non-collinear optical parametric amplifier (NOPA). This allowed for probe light to be generated in the 525–825 nm range. For measurements from 1 ns to 1 ms, electronically delayed 600 ps FWHM excitation pulses (≈0.25 mm^2 spot, 40 nJ per pulse) were provided by a frequency-doubled Q-switched Nd:YVO_4 laser (AOT-YVO-25QSPX, Advanced Optical Technologies). Every second pump pulse was omitted electronically. The pump and probe beams were focused to the same spot on the sample, then each probe pulse was detected and the differential transmission ($\Delta T/T$) calculated after accumulating and averaging 1500 "pump on" and "pump off" shots for each data point. Prior to striking the sample, a portion of the probe beam was split off as a reference beam and that was also passed through the sample and used to correct for shot-to-shot variation in the probe beam. Both the probe and reference beams enter a spectrometer (Princeton Instruments, Acton SpectraPro 2150i) offset vertically and are spectrally dispersed onto two 256-pixel photodiode arrays (Hamamatsu S3901256Q). Test samples consisted of 7 nm P3HT and 15 nm P(NDI2OD-T2), separated by 0–4 nm of PCDTBT interlayer, prepared on Spectrosil fused-silica following the methods described in "Photovoltaic Device Fabrication". Samples were measured in a vacuum chamber (10^{-5} mbar) at room temperature.

Pump-Push Photocurrent: A regenerative 1 kHz Ti:Sapphire amplifier system (Coherent, Legend Elite Duo) was used to pump both a broadband non-collinear optical amplifier (Clark) and a 3-stage home-built optical parametric amplifier (OPA) to generate visible pump pulses (600 ± 20) and infrared push pulses (2200 ± 100 nm) respectively. Reference photocurrent from a photodiode was detected at a pump repetition frequency of 1 kHz by a lock-in amplifier. The push beam was mechanically chopped at ≈380 Hz and its effect on the photocurrent was detected by a lock-in amplifier. ≈0.7 nJ pump and ≈1 μJ push pulses were focused into ≈1 mm^2 spot on the device. Pump-push transients contained an oscillatory coherent artifact contribution at negative delay times, which was fitted and fit-subtracted in exactly the same way from all the presented transients. Intensity dependence of the signal was measured and checked for multi-photon contributions. Test samples consisted of encapsulated photovoltaic devices fabricated using the previously described methods.

Supporting Information

Supporting Information is available from the Wiley Online Library or from the author.

Acknowledgements

We thank the EPSRC (UK) for financial support. Z.K.T. thanks the Singapore National Research Foundation (Energy Innovation Programme Office) for the research scholarship. A.A.B. acknowledges a VENI grant from the Netherlands Organization for Scientific Research (NWO). A.A.B. thanks Huib Bakker for providing laser facilities.

Received: January 16, 2013
Revised: March 12, 2013
Published online: June 12, 2013

[1] H. Treutlein, K. Schulten, A. T. Brünger, M. Karplus, J. Deisenhofer, H. Michel, *Proc. Natl. Acad. Sci. USA* **1992**, *89*, 75.
[2] D. A. LaVan, J. N. Cha, *Proc. Natl. Acad. Sci. USA* **2006**, *103*, 5251.
[3] R.-Q. Png, P.-J. Chia, J.-C. Tang, B. Liu, S. Sivaramakrishnan, M. Zhou, S.-H. Khong, H. S. O. Chan, J. H. Burroughes, L.-L. Chua, R. H. Friend, P. K. H. Ho, *Nat. Mater.* **2010**, *9*, 152.
[4] A. Tada, Y. Geng, Q. Wei, K. Hashimoto, K. Tajima, *Nat. Mater.* **2011**, *10*, 450.
[5] J. J. M. Halls, C. A. Walsh, N. C. Greenham, E. A. Marseglia, R. H. Friend, S. C. Moratti, A. B. Holmes, *Nature* **1995**, *376*, 498.
[6] G. Yu, J. Gao, J. C. Hummelen, F. Wudl, A. J. Heeger, *Science* **1995**, *270*, 1789.
[7] J. J. M. Halls, J. Cornil, D. A. dos Santos, R. Silbey, D. H. Hwang, A. B. Holmes, J. L. Brédas, R. H. Friend, *Phys. Rev. B* **1999**, *60*, 5721.
[8] V. D. Mihailetchi, H. X. Xie, B. de Boer, L. J. A. Koster, P. W. M. Blom, *Adv. Funct. Mater.* **2006**, *16*, 699.
[9] C. G. Shuttle, B. O'Regan, A. M. Ballantyne, J. Nelson, D. D. C. Bradley, J. R. Durrant, *Phys. Rev. B* **2008**, *78*, 113201.
[10] L. J. A. Koster, E. C. P. Smits, V. D. Mihailetchi, P. W. M. Blom, *Phys. Rev. B* **2005**, *72*, 085205.
[11] V. D. Mihailetchi, L. J. A. Koster, J. C. Hummelen, P. W. M. Blom, *Phys. Rev. Lett.* **2004**, *93*, 216601.
[12] S. Westenhoff, I. A. Howard, J. M. Hodgkiss, K. R. Kirov, H. A. Bronstein, C. K. Williams, N. C. Greenham, R. H. Friend, *J. Am. Chem. Soc.* **2008**, *130*, 13653.
[13] J. M. Hodgkiss, A. R. Campbell, R. A. Marsh, A. Rao, S. Albert-Seifried, R. H. Friend, *Phys. Rev. Lett.* **2010**, *104*, 177701.
[14] R. A. Marsh, J. M. Hodgkiss, R. H. Friend, *Adv. Mater.* **2010**, *22*, 3672.
[15] L. J. A. Koster, V. D. Mihailetchi, P. W. M. Blom, *Appl. Phys. Lett.* **2006**, *88*, 052104.
[16] C. G. Shuttle, R. Hamilton, B. C. O'Regan, J. Nelson, J. R. Durrant, *Proc. Natl. Acad. Sci. USA* **2010**.
[17] A. A. Bakulin, S. A. Zapunidy, M. S. Pshenichnikov, P. H. M. van Loosdrecht, D. Y. Paraschuk, *Phys. Chem. Chem. Phys.* **2009**, *11*, 7324.
[18] N. Li, F. Machui, D. Waller, M. Koppe, C. J. Brabec, *Sol. Energy Mater. Sol. Cells* **2011**, *95*, 3465.
[19] P. P. Khlyabich, B. Burkhart, B. C. Thompson, *J. Am. Chem. Soc.* **2011**, *133*, 14534.
[20] S. Honda, S. Yokoya, H. Ohkita, H. Benten, S. Ito, *J. Phys. Chem. C* **2011**, *115*, 11306.
[21] M. Schubert, D. Dolfen, J. Frisch, S. Roland, R. Steyrleuthner, B. Stiller, Z. Chen, U. Scherf, N. Koch, A. Facchetti, D. Neher, *Adv. Energy Mater.* **2012**, *2*, 369.
[22] C. Goh, S. R. Scully, M. D. McGehee, *J. Appl. Phys.* **2007**, *101*, 114503.
[23] P. E. Shaw, A. Ruseckas, I. D. W. Samuel, *Adv. Mater.* **2008**, *20*, 3516.
[24] A. Kahn, N. Koch, W. Gao, *J. Polym. Sci. Pol. Phys.* **2003**, *41*, 2529.
[25] Y. Vaynzof, D. Kabra, L. Zhao, L. L. Chua, U. Steiner, R. H. Friend, *ACS Nano* **2010**, *5*, 329.
[26] L.-H. Zhao, R.-Q. Png, J.-M. Zhuo, L.-Y. Wong, J.-C. Tang, Y.-S. Su, L.-L. Chua, *Macromolecules* **2011**, *44*, 9692.

[27] L. A. A. Pettersson, L. S. Roman, O. Inganas, *J. Appl. Phys.* **1999**, *86*, 487.
[28] P. Peumans, A. Yakimov, S. R. Forrest, *J. Appl. Phys.* **2003**, *93*, 3693.
[29] J. Guo, H. Ohkita, H. Benten, S. Ito, *J. Am. Chem. Soc.* **2010**, *132*, 6154.
[30] M. Caironi, M. Bird, D. Fazzi, Z. Chen, R. Di Pietro, C. Newman, A. Facchetti, H. Sirringhaus, *Adv. Funct. Mater.* **2011**, *21*, 3371.
[31] J. R. Moore, S. Albert-Seifried, A. Rao, S. Massip, B. Watts, D. J. Morgan, R. H. Friend, C. R. McNeill, H. Sirringhaus, *Adv. Energy Mater.* **2011**, *1*, 230.
[32] R. H. Friend, M. Phillips, A. Rao, M. W. B. Wilson, Z. Li, C. R. McNeill, *Faraday Discuss.* **2012**, *155*, 339.
[33] A. A. Bakulin, A. Rao, V. G. Pavelyev, P. H. M. van Loosdrecht, M. S. Pshenichnikov, D. Niedzialek, J. Cornil, D. Beljonne, R. H. Friend, *Science* **2012**, *335*, 1340.
[34] Y. Vaynzof, A. A. Bakulin, S. Gélinas, R. H. Friend, *Phys. Rev. Lett.* **2012**, *108*, 246605.
[35] Y. Kinoshita, T. Hasobe, H. Murata, *Appl. Phys. Lett.* **2007**, *91*, 083518.
[36] S. Sista, Y. Yao, Y. Yang, M. L. Tang, Z. Bao, *Appl. Phys. Lett.* **2007**, *91*, 223508.
[37] C. W. Schlenker, V. S. Barlier, S. W. Chin, M. T. Whited, R. E. McAnally, S. R. Forrest, M. E. Thompson, *Chem. Mater.* **2011**, *23*, 4132.
[38] T. D. Heidel, D. Hochbaum, J. M. Sussman, V. Singh, M. E. Bahlke, I. Hiromi, J. Lee, M. A. Baldo, *J. Appl. Phys.* **2011**, *109*, 104502.
[39] M.-S. Kim, J.-S. Kim, J. C. Cho, M. Shtein, L. J. Guo, J. Kim, *Appl. Phys. Lett.* **2007**, *90*, 123113.
[40] M. Aryal, F. Buyukserin, K. Mielczarek, X.-M. Zhao, J. Gao, A. Zakhidov, W. Hu, *J. Vac. Sci. Technol. B* **2008**, *26*, 2562.
[41] X. He, F. Gao, G. Tu, D. Hasko, S. Hüttner, U. Steiner, N. C. Greenham, R. H. Friend, W. T. S. Huck, *Nano Lett.* **2010**, *10*, 1302.